*PTI Journal* *Technical Paper*

# MONITORING SECONDARY MOMENTS OF CONTINUOUS UNBONDED POST-TENSIONED CONCRETE BEAMS

By
KYUNGMIN KIM AND THOMAS H.-K. KANG

POST-TENSIONING INSTITUTE ®

Authorized reprint from: December 2018 issue of the PTI Journal

# MONITORING SECONDARY MOMENTS OF CONTINUOUS UNBONDED POST-TENSIONED CONCRETE BEAMS

BY KYUNGMIN KIM AND THOMAS H.-K. KANG

*Experiments on flexural behavior of three two-span unbonded post-tensioned (PT) beams were conducted under four-point static loading condition. A detailed investigation on internal moment and secondary moment at critical sections was carried out and is discussed in this paper. Observations conducted as part of this experimental research surprisingly revealed that the experimentally obtained secondary moment in the specimens was significantly larger than that predicted using indeterminate frame analysis and the load-balancing method, particularly at the ultimate limit state. Details pertaining to the procedure in which secondary moment from the measured data was obtained and its review are provided in this paper.*

## KEYWORDS:

continuous beam; experimental study; indeterminate structure; post-tensioned concrete; secondary moment; unbonded tendon.

## INTRODUCTION

In continuous post-tensioned (PT) beams with non-concordant tendon profiles, prestressing force deforms members such that restricted deformation at the supports produces secondary reactions. The secondary reactions act as external forces to the member, which induce secondary moments. The concept of secondary moments in continuous prestressed concrete beams had been achieved in the late twentieth century. According to ACI 318-71 (ACI Committee 318 1971), secondary moments were to be neglected in flexural strength calculations. The presumption was that secondary moments became nonexistent upon plastic hinge formation at the interior supports. The requirement to include secondary moments in strength calculations first appeared in ACI 318-77 (ACI Committee 318 1977). The moment used in calculating required strength is the sum of the moments due to factored loads and the secondary moment with an applied load factor of 1.0.

In continuous prestressed concrete structures, secondary moment can contribute to reduction in negative moment demand at the interior supports but can also increase moment demand in positive moment regions of continuous members at midspan. Secondary action also affects column loads at both interior and exterior columns.

Member behavior from the viewpoint of the secondary moment at the serviceability limit state was studied by Wyche et al. (1992). Literature review conducted by Cohn and Frostig (1983), however, stated that depending on the different approaches, the secondary moments in the post-elastic range showed different variation trends at various loading stages—some remained constant, others increased, decreased, or even disappeared. A limited number of experimental studies of continuous unbonded PT one-way members with two spans or more were carried out by prior researchers (Burns and Pierce 1967; Burns et al. 1991; Maguire et al. 2016). The objective of tests conducted by Burns and Pierce (1967) was to investigate the effect of bonded reinforcement and influential variables for ultimate capacity, while Burns et al. (1991) studied the redistribution of tendon force and member strength. The center support reaction force was monitored by Burns et al. (1991). However, there were no actuator-applied load values reported in the literature. Maguire et al. (2016) also did not measure the support reaction in their two-spanned PT slab tests. Lin (1955) conducted monotonic and repeated loading tests of two-spanned bonded PT beams and measured the support reaction; however, the behavior of bonded systems may be different from that of unbonded systems. Accordingly, there have been limited quantitative studies revealing the nature of the secondary moment in various behavioral zones of "unbonded" PT structures. Particularly, no experimental studies monitored secondary reactions and associated moments in the post-elastic range.

To obtain better insight into secondary moment behavior of continuous unbonded PT concrete beams, an experimental study was conducted using two-span contin-

*PTI JOURNAL*, V. 14, No. 2, December 2018. Received and reviewed under Institute journal publication policies.  Pertinent discussion will be published in the next issue of *PTI JOURNAL* if received within 3 months of the publication.

uous PT beams with three simple supports. Two test variables were considered in the experiment: prestressing force magnitude and tendon profile height. Results of this experimental investigation are presented in this paper, with emphasis on secondary moment monitoring.

## EXPERIMENTAL PROGRAM

To investigate the flexural behavior of PT members along with associated secondary moment behavior, a large-scale experiment was carried out using a total of three two-span unbonded PT beams. The specimens were designed based on the continuous PT beams used in an existing building constructed in 2015 in Korea. The scale of the specimens was reduced to half due to experimental site limitations. Two test variables, profile height and prestressing force magnitude, were considered and accommodated in the specimen design. The half-scaled specimens were designed and checked following ACI 318-14 (ACI Committee 318 2014) and PTI M50.2-00 (PTI Committee M-50 2000), as well as KCI-12 (KCI 2012). Figures 1 and 2 show dimensions and details of the test specimens. The two-span continuous beams had a 400 x 450 mm (15.7 x 17.7 in.) section and 14.6 m (47.9 ft) total length with a cantilever of 450 mm (17.7 in.) on each end. Every specimen lay symmetric about the interior support and tendon profile followed parabolic curves shown in Fig. 3.

Concrete with a specified compressive strength of 50 MPa (7250 psi) was used in fabrication of the specimens and allowed to cure for 40 days prior to being subject to jacking and load testing forces. Reinforcing bars used were: D16, D13, and D10 ($d_b$ = 16, 13, and 10 mm [0.6, 0.5, and 0.4 in.], respectively). For unbonded post-tensioning reinforcement, high-density polyethylene (HDPE)-sheathed seven-wire strands with 1860 MPa (270 ksi) tensile strength and a diameter of 15.2 mm (0.6 in.) was used. One strand for Specimen 4L or 4H was manually inserted into an HDPE tube with grease applied on the strand surface to see the difference of friction characteristics. The other three strands for Specimen 4L or 4H and all strands for Specimen 5L were prefabricated extruded single-strand tendons available in a plant. Information about the specimens, including material properties, are summarized in Table 1. The specimens are denoted 4H, 4L, and 5L, where the first digit indicates the number of single-strand tendons in the specimen and the last letter, H or L, stands for the high or low profile, respectively. The specimens were fabricated and jacked in a precast concrete plant (no pre-tensioning is applied), and the fabrication procedure is presented in Fig. 4.

The specimens, illustrated in Fig. 2, were seated on three round cylindrical supports. Two hydraulic actua-

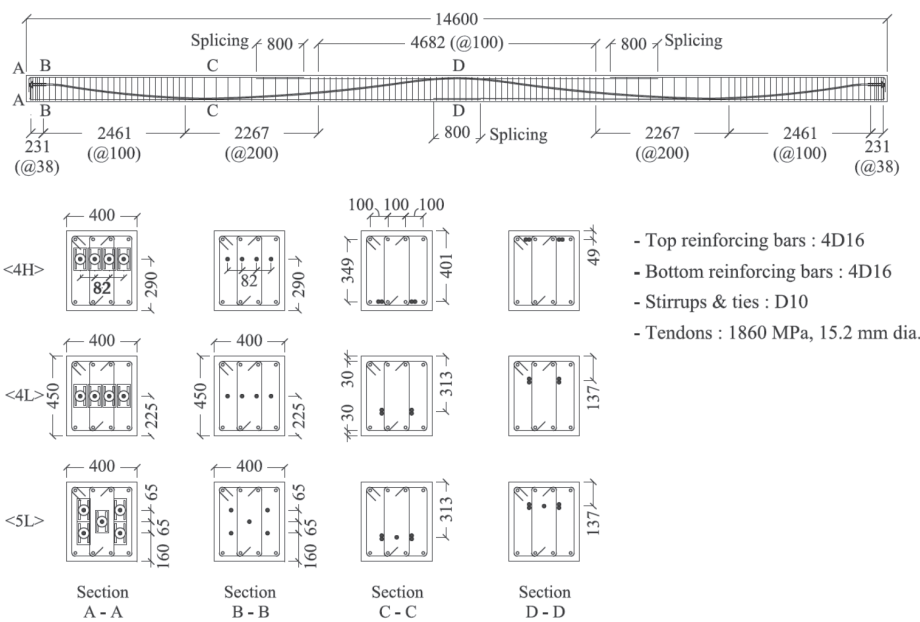


*Fig. 1—Specimen details. (Note: Units in mm and MPa; 1 in. = 25.4 mm; 1 MPa = 145 psi.)*

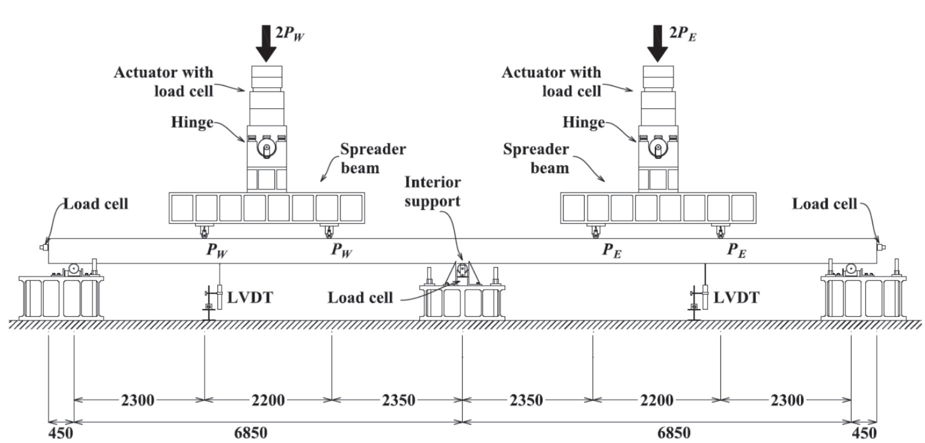


*Fig. 2—Two-span beam tests. (Note: Units in mm; 1 in. = 25.4 mm.)*

tors were used to apply quasi-static loads individually on both spans and at the same rate of displacement control (1 mm/min [0.4 in./min]). Two spreader beams were attached at the end of each actuator connected with rotatable hinges. Because the spreader beams were rotatable with respect to its connection, the actuator load was equally divided and transferred to the two loading points of each span: two $P_E$ values on the east span and two $P_W$ values on the west span. This setup allowed for mimicking of the internal moment diagram associated with a uniformly distributed load as much as possible.

Post-tensioning was applied prior to seating the beam specimen on top of three supports. By using hollow-core load cells at the jacking and fixed ends, prestressing force of a representative tendon was measured throughout the loading testing of each specimen. Each actuator had a built-in load cell that measured the applied load. In addition to the load cells in the actuators, an additional 200-ton-capacity load cell was employed under the interior support so that the elastic and plastic behavior of the indeterminate structure could be investigated. Linear variable displacement transducers (LVDTs) were installed to measure vertical deflections where the maximum deflection was expected.

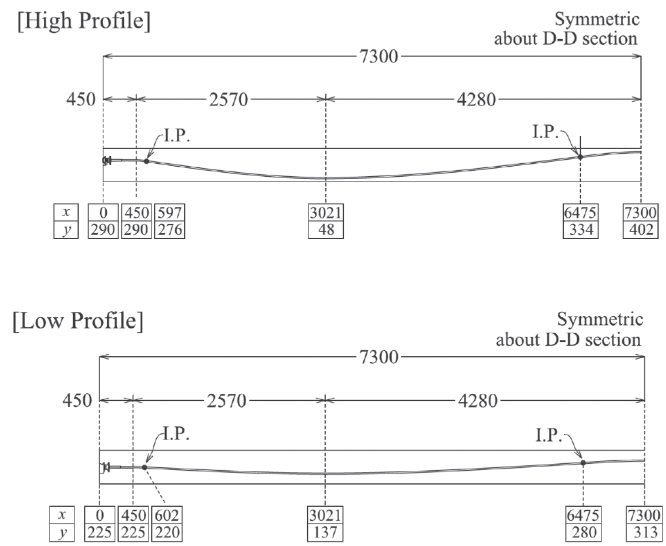


*Fig. 3—Profile shape and location at select points. (Note: Units in mm; 1 in. = 25.4 mm; I.P. is inflection point of tendon curvature.)*

**Table 1—Test specimen details**

| Specimen | 4H | 4L | 5L |
|---|---|---|---|
| Specified tensile strength of strands, MPa | 1860 | 1860 | 1860 |
| Number of strands | 4 | 4 | 5 |
| $h_p$, mm | 354 | 176 | 176 |
| $f_{se}$, MPa | 1237.5 | 1239.4 | 1239.4 |
| $f_c'$, MPa | 52.7 | 52.7 | 52.7 |
| $f_y$, MPa | 478.2 | 478.2 | 478.2 |
| $A_s$, mm$^2$ | 799.4 | 799.4 | 799.4 |
| $A_{ps}$, mm$^2$ | 277.4 | 554.8 | 693.5 |
| ρ, % | 0.22 | 0.44 | 0.44 |
| $\rho_p$, % | 0.35 | 0.44 | 0.55 |
| $b$, mm | 400 | 400 | 400 |
| $d$, mm | 450 | 450 | 450 |
| $l$, m | 6.85 | 6.85 | 6.85 |
| $d_s$, mm | 402 | 402 | 402 |
| $d_p$, mm | 402 | 313 | 313 |

Note: $h_p$ is vertical distance of tendon profile measured from center of highest point to center of lowest point; $f_{se}$ is effective stress in post-tensioning reinforcement, after allowance for all prestress losses; $f_c'$ is measured compressive strength of concrete; $f_y$ is measured yield strength for nonprestressed mild steel reinforcement; $A_s$ is area of nonprestressed longitudinal tension reinforcing bars; $A_{ps}$ is area of post-tensioning tendons; ρ is ratio of $A_s$ to $bd_s$; $\rho_p$ is ratio of $A_{ps}$ to $bd_p$; b is section width; $d$ is section depth; l is span net length; $d_s$ is distance from extreme compression fiber to centroid of longitudinal tension reinforcing bars; $d_p$ is distance from extreme compression fiber to centroid of post-tensioning tendons; 1 MPa = 145 psi; 1 in. = 25.4 mm.

## PRESTRESS DISTRIBUTION DUE TO FRICTION

The tendons were tensioned to approximately 75% of their specified tensile strength. After short- and long-term losses, approximately $0.65f_{pu}$ remained on average as effective prestress. Prestress in the tendon is not the same throughout the length of the member due to friction and anchor-set loss. To observe differences in friction characteristics, a tendon was chosen in each specimen to measure prestress at its jacking and fixed ends.

Figure 5 shows prestress variation of the representative tendon during jacking in Specimen 4H. In the figure, the discrepancy between the jacking and fixed ends, presented as "friction loss," is the total friction loss due to curvature friction and wobble friction. Pure friction loss between the two ends was measured prior to anchor-set loss when the monostrand jack held the strand.

The prestress loss due to anchor set and long-term loss is presented in Fig. 5. By using the following Eq. (1), which is provided in ACI 423.10R-16, and the measured prestress, the curvature friction coefficient and the wobble friction coefficient were calculated.

$$T_x = T_0 e^{-(\mu\alpha + \kappa x)} \tag{1}$$

where $x$ is the length of tendon from jacking end to point $x$; $T_x$ is the prestressing force at point $x$; $\mu$ is the curvature friction coefficient; $\kappa$ is the wobble friction coefficient; and $\alpha$ is the total angular change in radians from jacking end to point $x$ (1.047 radians for high-profiled specimens of 4H and 0.628 radians for low-profiled specimens of 4L and 5L in total).

It is noted that the friction observed was larger in the tightly extruded single-strand tendons than in the manually inserted strand tendons. Assuming curvature coefficient was constant, wobble friction coefficient of the manually inserted tendons was approximately half of that of the tendons, which were manufactured in the plant.

Figure 6 shows the prestress variation profile for each tendon after the anchor set loss. Anchor set losses were considered to be the same for all tendons because the same anchorages and wedges were used throughout. Friction loss was also assumed to be linear (that is, the total angular change was divided by the total length). Once friction was calculated based on the data, stress distribution was drawn on the basis of the average measured value at the jacking end. Because the wobble coefficient of the extruded tendon was larger than the manually fabricated tendon, the slopes of the prestress distribution diagram of extruded tendons were also steeper.

The averaged prestress distribution for the tendons in each specimen is shown in Fig. 7. To make the specimens as

*(a) Tendon profile shaping*

*(b) Concrete pouring*

*(c) Steam curing*

*(d) Removing formwork*

*(e) Jacking strands*

*(f) Completion*

*Fig. 4—Fabrication process.*

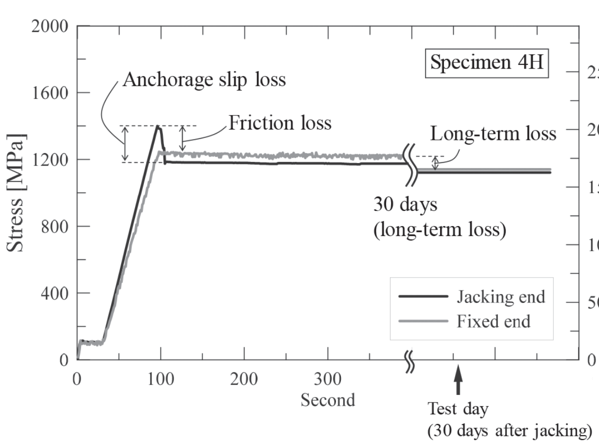


*Fig. 5—Prestress variation from jacking to loading test at jacking and fixed ends (Specimen 4L).*

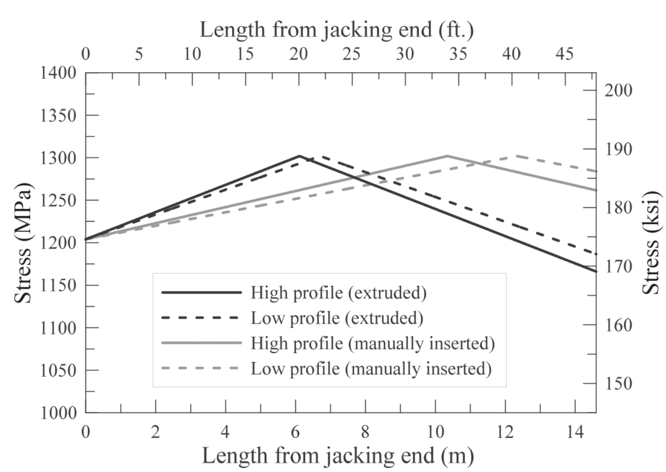


*Fig. 6—Prestress variation profile.*

symmetric as possible about the interior support, the locations of the jacking and fixed ends were switched between both ends (that is, alternated jacking). Figure 7 shows the curve shifting downward or upward in the y-axis direction due to the long-term loss or increase in prestress ($\Delta f_{ps}$) up to the point where the peak load was measured. Prestress increases monitored at both the jacking and fixed ends were quite close.

## STATICS ANALYSIS

Because of the characteristics of structural indeterminacy in two-span PT beams, it is not possible to directly obtain the reaction force at all supports ($L$, $R_E$, and $R_W$), even though the magnitude of the loads applied from the actuators ($P_E$ and $P_W$) are known. Here, $L$ is the measured reaction force at the interior support; $R_E$ and $R_W$ are the reaction forces at the end support on the east and west sides, respectively; and $P_E$ and $P_W$ are the half of the actuator force on the east and west sides, respectively. By using the load cell data ($L$) under the interior support, $R_E$ and $R_W$ can be obtained. With the derived reactions at the end supports, internal moments at the critical sections and any other sections can also be obtained. Here, maximum negative moment occurs at the interior support with maximum positive moments on the east and west spans are anticipated. Plastic hinges are considered to occur at these critical sections. At the interior support location, the first plastic hinge formed. Maximum positive moment on each span formed the second hinges. All three specimens have the same section geometry with the exception of tendon location.

Equations (2), (3), and (4) show the equilibrium regarding the reaction forces, and Fig. 8(a) provides an illustration. Equations (5) through (9) show how internal moments at critical sections were derived using the method of sections in statics analysis (refer to Fig. 8(b)).

$$2P_E + 2P_W + w(= 4.32\ \text{kN/m}) \times (14.6\ \text{m}) = L + R_E + R_W \tag{2}$$

$$R_E = 0.5P_W + 1.5P_E - 0.5L + 31.5 \tag{3}$$

$$R_W = 0.5P_E + 1.5P_W - 0.5L + 31.5 \tag{4}$$

$$V_1 = 0.5L + 0.5(P_E - P_W) \tag{5}$$

$$V_2 = 0.5P_W + 0.5P_E - 0.5L + 19.7 \tag{6}$$

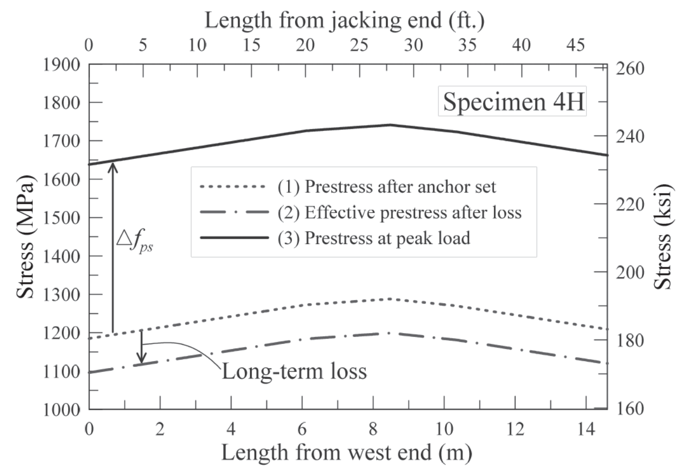


*(a) Averaged prestress distribution (Specimen 4H)*

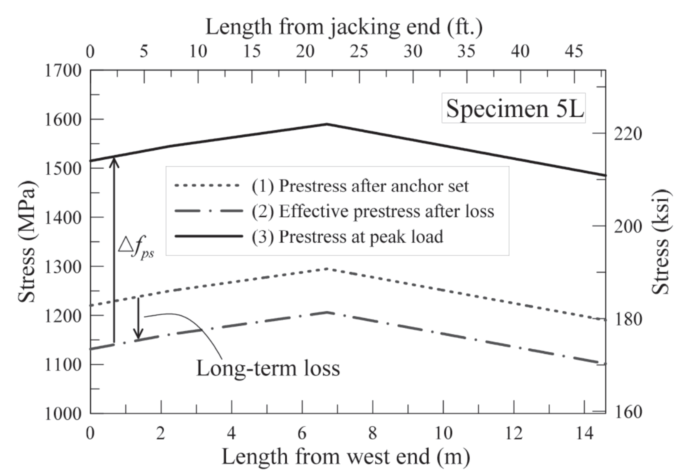


*(b) Averaged prestress distribution (Specimen 4L)*

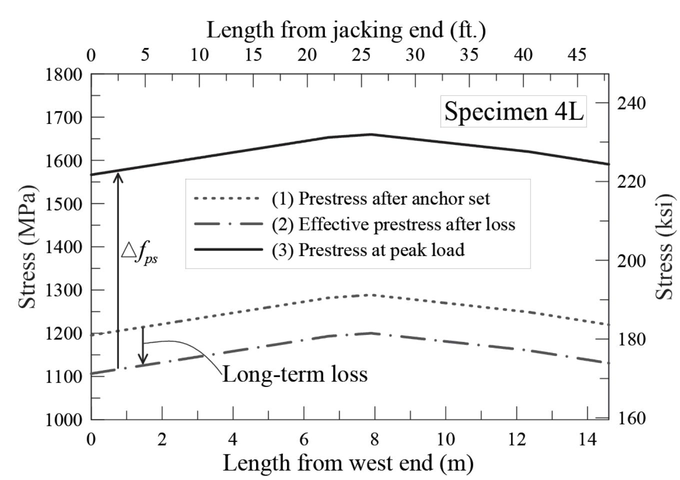


*(c) Averaged prestress distribution (Specimen 5L)*

*Fig. 7—Averaged prestress distributions.*

$$M_I = 3.4P_E + 3.4P_W - 3.43L + 100.9 \quad (7)$$

$$M_E = 1.14P_W + 3.46P_E - 1.15L + 56.2 \quad (8)$$

$$M_W = 1.14P_E + 3.46P_W - 1.15L + 56.2 \quad (9)$$

where $P_E$ is the half of the actuator force on the east side (kN); $P_W$ is the half of the actuator force on the west side (kN); $w$ is the uniform line load of self-weight applied throughout the beam (kN/m); $L$ is the measured reaction force at the interior support (m); $R_E$ is the reaction force at the end support on the east side (kN); $R_W$ is the reaction force at the end support on the west side (kN); $V_1$ and $V_2$ are the shear forces in the sections represented in Fig. 8(b)(kN); $M_I$ is the internal moment at the interior support location obtained using the load cell data (kN-m); and $M_E$ and $M_W$ are the internal moment based on the load cell data at the maximum positive moment locations, 4.55 m (14.9 ft) east and west of the interior support, respectively (kN-m). Note that to maintain accuracy, load cells were calibrated before and after the loading test.

Internal moment variation for Specimen 4L is presented in Fig. 9 as an example. In the figure, the absolute value of $M_I$ is plotted for comparison with $M_E$ and $M_W$. Because the section at the interior support and the critical sections on the spans are symmetrical with respect to the middepth of the beam section, the nominal moment strengths ($M_n$) at all plastic hinging regions are expected to be the same. However, Fig. 9 clearly shows that internal moment at the interior support ($M_I$) was much smaller than the calculated $M_n$ value, despite the earlier formation of plastic hinging at this location. As such, there was also significant discrepancy between $M_I$ and $M_E$ or $M_W$. Because measured reaction at the interior support did not increase significantly albeit increased total loading, this discrepancy may be attributed to the secondary effect.

As external loading $[2(P_E + P_W)]$ increased, hold-down force began to be generated at the interior support location and the reaction ($L$) did not increase much beyond the deflection of approximately 15 mm (0.6 in.) (Fig. 10). The data indicate that interior support reaction was redistributed to end supports. This observation differed from the posture that no secondary reactions or moments would be present because the beam was placed on top of the supports after post-tensioning and prior to the loading test (that is, no upward restraint). More details are provided in the following sections.

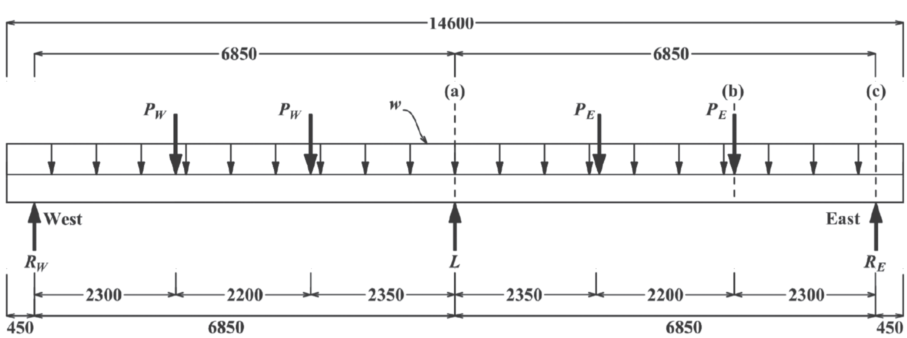


*(a) Free body diagram of specimen*

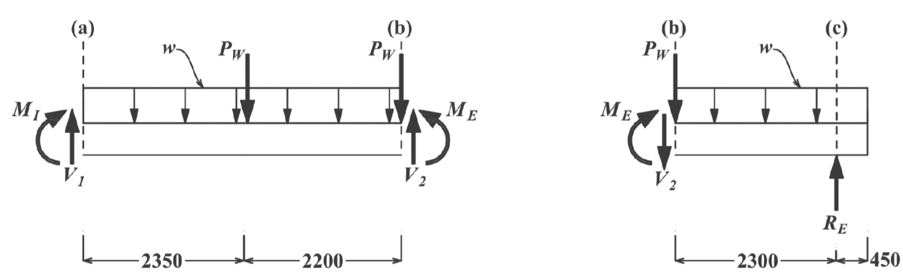


*(b) Free body diagrams of east parts using method of sections*

*Fig. 8—Free body diagrams. (Note: Units in mm; 1 in. = 25.4 mm.)*

## ESTIMATION OF SECONDARY MOMENT USING EXPERIMENTAL DATA

Secondary moment at a particular section of a member can be calculated by using the conventional indirect method shown in Eq. (10)

$$M_{2calc} = M_{bal} - M_1 \quad (10)$$

where $M_{2calc}$ is the calculated secondary moment at a particular section of the member using indeterminate frame analysis and the load-balancing method with exact tendon profile (not simplified ω-shaped profile with kink); $M_{bal}$ is the balanced moment by equivalent prestressing-induced force to concrete; $M_1$ is the primary moment that is calculated as $Pe$; $P$ is the prestressing force at the section of interest; and $e$ is the

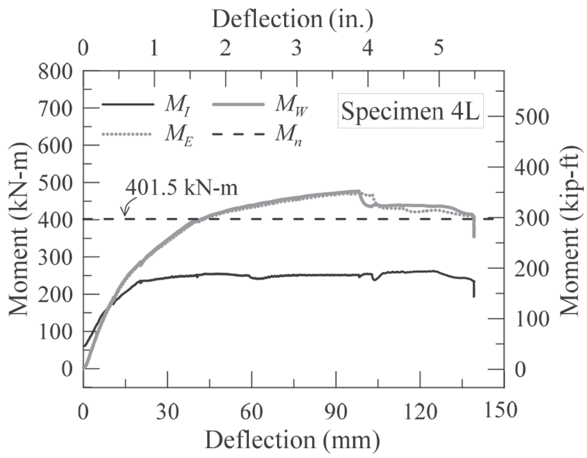


Fig. 9—Moment-deflection curves at critical sections in Specimen 4L ($M_I$, $M_E$, and $M_W$ = monitored internal moments at interior support, east midspan, and west midspan; $M_n$ = nominal positive or negative moment strength of 401.5 kN-m (296 ft-k) of any section calculated using Whitney stress block, measured $f_c'$ and $f_y$, and tendon stress at peak load at interior support [refer to Fig. 7]).

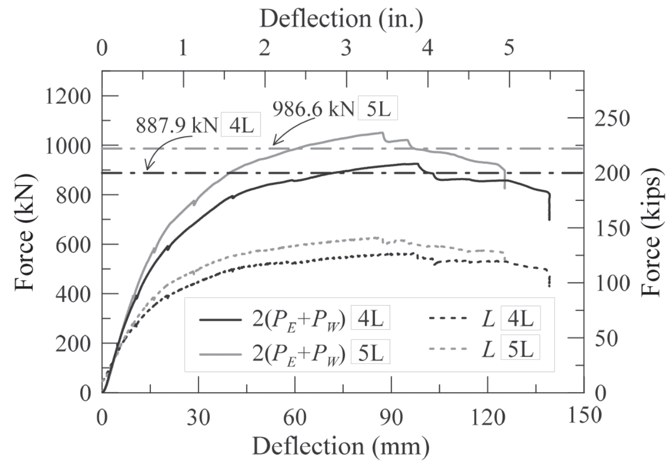


Fig. 10—Load-deflection curves based on measured total actuator load ($2P_E + 2P_W$) or measured interior support reaction (L) for Specimens 4L and 5L.

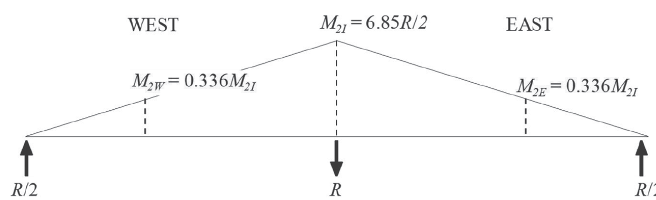


Fig. 11—Secondary moment diagram. (Note: Units in kN-m; 1 kN-m = 738 ft-lb.)

eccentricity from c.g.c. (center of gravity of concrete) to c.g.s. (center of gravity of prestressing steel).

However, it was observed from the experimental results that there was a significant discrepancy between actual member behavior and calculated values from Eq. (10). Assuming that the secondary moment is produced by the secondary reaction forces represented as $R$ at the interior support and $R/2$ at the end supports as shown in Fig. 11, the secondary moment diagram can be drawn as a triangular shape. In the figure, $M_{2I}$ is the secondary moment at the interior support location, and $M_{2E}$ and $M_{2W}$ are the secondary moments at the maximum positive moment sections on the east and west spans, respectively. The experimental result of internal moment was assumed to include both gravity moment and secondary moment. Using the geometrical feature of the secondary moment diagram (Fig. 11), the absolute value of internal (negative) moment ($M_I$) is the difference between the gravity (negative) moment and $M_{2I}$ (positive). Note that the difference is taken because the signs of the moments are opposite. In the same manner, $M_E$ or $M_W$ is the internal (positive) moment, the gravity (positive) moment at the section plus $0.336M_{2I}$ (positive). The value of $0.336M_{2I}$ is the secondary moment at the outer loading point on the beam, where the largest gravity moment is expected (that is, critical section), given the value of $M_{2I}$ at the interior support (refer to Fig. 11). Only, the secondary effect can explain the discrepancy between the values of $M_I$ and $M_{2E}$ (or $M_{2W}$) shown in Fig. 9.

In the following subsections, the methodology of estimating the secondary moment is presented depending on the state of the section at the interior support location. The monitored internal moment of $M_I$ was divided into three different behavioral zones (elastic, transition, and plastic; refer to Fig. 12).

## Estimation of secondary moment in elastic zone using experimental data

The elastic zone of $M_I$ can be identified as the range where the internal moment ($M_I$) shows a direct proportional relationship with deflection. In this range, secondary moment can be calculated by using the discrepancy between the (negative) moment applied by self-weight and actuator and $M_I$ (positive). The moment by self-weight and actuator is assumed to be proportional to the measured deflection prior to cracking as shown in Eq. (11). Note that the first and second terms of the left-hand side of the equation have different signs (negative and positive, respectively) and $M_I$ is negative.

$$M_{cr} \frac{\Delta_x}{\Delta_{cr}} + M_{2I} = M_I \ \text{(kN-m)} \tag{11}$$

where $M_{cr}$ is the (negative) moment required to make the first crack at the interior support section without consideration of secondary moment; $\Delta_x$ is the displacement generated by the actuator load in the measured moment-deflection curve; $\Delta_{cr}$ is the total deflection at first cracking in the measured moment-deflection curve (refer to Fig. 12); $M_{2I}$ is the (positive) secondary moment; and $M_I$ is the measured (negative) moment using Eq. (7).

$M_{cr}$ can be defined using the following equation

$$M_{cr} = -\left\{Pe + \frac{I}{y}(f_r + P/A_{tr})\right\} = -65.7 - kP \text{ (kN-m)} \quad (12)$$

where $P$ is the monitored post-tensioning force at the interior support location (refer to Fig. 7); $e$ is the eccentricity of the tendon at the interior support location; $I$ is the moment of inertia of the transformed section of concrete; $f_r$ is the modulus of rupture calculated using the measured concrete strength and the formula provided by ACI 318-14; $A_{tr}$ is the sectional area of the transformed concrete section; $y$ is the distance between c.g.c. and the extreme tension fiber of the interior support section; and $k$ is the constant which is 0.255 for the specimens with high tendon profile and 0.166 for low tendon profile.

## Estimation of secondary moment in plastic zone using experimental data

Plastic zone is identified as the range where the increase rate of $M_I$ substantially drops and shows a trend

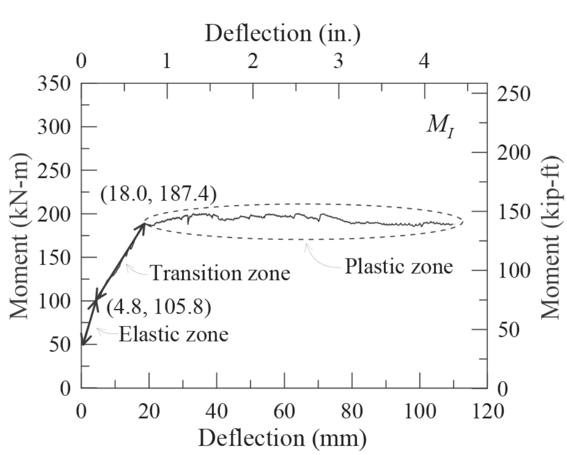


*Fig. 12—Behavior zone identification of Specimen 4H from internal moment at interior support ($M_I$) versus deflection relationship.*

of plastic hinging (Fig. 12). In this range, the secondary moment can be calculated by taking the difference between the (negative) plastic moment calculated based on $f_p$ and the monitored $M_I$ (negative) at every step, where $f_p$ is the tendon stress at the interior support location at each load step (refer to Fig. 7) and all mild steel reinforcing bars have yielded in the plastic zone. This is presented in Eq. (13)

$$M_{@fp} + M_{2I} = M_I \text{ (kN-m)} \quad (13)$$

where $M_{@fp}$ is the (negative) plastic moment at the interior support location estimated based on the monitored $f_p$; $M_{2I}$ is the (positive) secondary moment; and $M_I$ is the measured (negative) moment using Eq. (7).

Here, $M_{@fp}$ is estimated using Eq. (14) and (15)

$$M_{@fp} \cong -\left\{f_y A_s\left(d_s - \frac{a}{2}\right) + f_p A_{ps}\left(d_p - \frac{a}{2}\right)\right\} \text{ (kN-m)} \quad (14)$$

$$a = \frac{f_p A_{ps} + f_y A_s}{0.85 f_c' b} \text{ (m)} \quad (15)$$

where $f_y$ is the measured yield strength of nonprestressed mild steel reinforcement; $A_s$ is the area of nonprestressed longitudinal tensile reinforcement; $d_s$ is the distance from extreme compression fiber to the centroid of nonprestressed longitudinal tensile reinforcement; $f_p$ is the monitored tendon prestress (refer to Fig. 7); $A_{ps}$ is the area of post-tensioning reinforcement; $d_p$ is the distance from the extreme compression fiber to the centroid of post-tensioning reinforcement; $f_c'$ is the measured compressive strength of concrete; and $b$ is the width of the specimen. It is clearly notable in Fig. 10 that the measured total actuator load exceeded the plastic capacity of the whole member calculated through the plastic analysis theory, where the nominal moment strengths ($M_n$) were assumed to be reached at two positive moment regions (at midspan) and two negative moment regions (at interior support) based on the general collapse mechanism. The values of 887.9 and 986.6 kN (200 and 222 kip) were calculated to be the plastic capacities of Specimens 4L and 5L, respectively, as represented by dot-dashed lines in Fig. 10. This kind of assumption is common for plastic design (Harajli et al. 2002; Lee et al. 2015).

### Estimation of secondary moment in transition zone using experimental data

The transition zone is linearly interpolated between the two points: the end point of the elastic zone and the beginning point of the plastic zone.

## OBSERVATION AND DISCUSSION

All specimens observed developed the first plastic hinge at the interior support, followed by development of the second plastic hinges on both spans. The photos of typical failure modes are presented in Fig. 13, and the secondary moment test results based on the methodology introduced in this paper are provided in Fig. 14, where $M_{2calc}$ is the calculated secondary moment using indeterminate frame analysis and load-balancing method as defined in Eq. (10).

The secondary support reaction and moment were calculated by using finite element computer software and the equivalent load by post-tensioning based on $f_p$ as well as based on the actual tendon profile (refer to Hufnagel and Kang [2012]) (not simplified ω-shaped profile with kink; refer to Fig. 4 in the paper by Bondy [2003]). The absolute value of $M_I$ (negative internal moment) is plotted for comparison purposes. In the figure, the secondary moments of Specimen 4H were evaluated assuming that there were only two tendons acting in the system because developed strength was representative of only two tendons and the monitored elastic shortening validated this assumption. The first jacked tendon measured, when compared to other specimens, experienced very small prestress loss due to the elastic shortening effect (refer to Table 2). The presumption is that two of the tendons unfortunately experienced dead-end wedge slip during the live end jacking operation. No push seating or pulling the wedges was made, nor were there any spring-loaded wedges. The moments including $M_{2calc}$ in Specimen 4H showed a sudden drop because the tendon used for monitoring $f_p$ in the specimen fractured at that point.

In addition, at the serviceability limit state but throughout the entire loading stages, $M_{2I}$ and $M_{2calc}$ show very different values. Initially, the $M_{2I}$ value was negative right after PT specimens were simply put on the supports. However, when load was applied, the (positive) secondary moment appeared to “activate” and indicated quite large increases for all specimens, whereas $M_{2calc}$ was calculated to be almost constant in the elastic zone, with slight increase as prestress increased and the member underwent the plastic range.

The results in this experimental study are quite surprising and differed from existing postulation. The larger the post-tensioning force, the larger the secondary moment (compare Fig. 7(b) and 7(c)). The comparison reveals that the secondary moment in the plastic range showed almost a proportional relationship with regard to the post-tensioning forces when the tendon profile shape was the same (refer to Table 3). Specimen 4H developed almost the same amount of secondary moment at its peak load compared to Specimen 4L, although 4H had only half the number of tendons of Specimen 4L. Based on experimental data observed, it can be inferred that higher tendon profiles in prestressed members produce larger secondary moments in the plastic range.

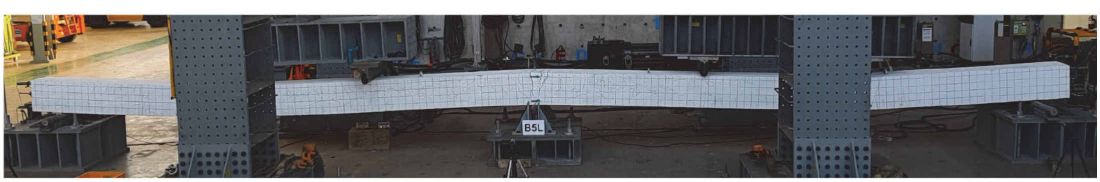


*(a) Overview of deformed specimen*

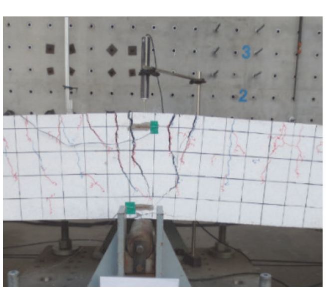

*(b) Plastic hinging at interior support location*

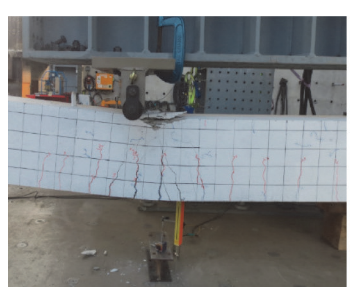

*(c) Plastic hinging at midspan location*

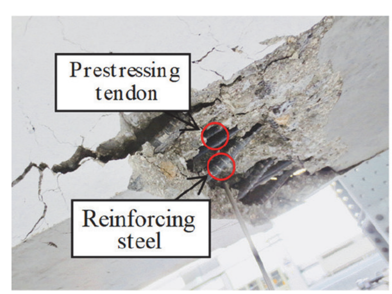


*(d) Tendons and reinforcing bars exposed*

*Fig. 13—Observed failure.*

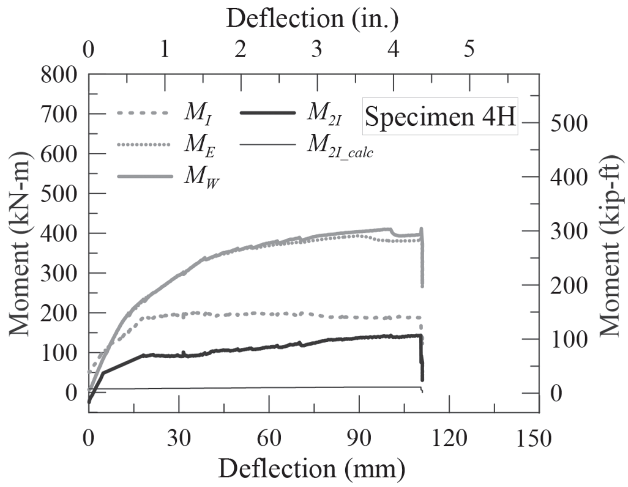


*(a) Internal moment-deflection curves of Specimen 4H*

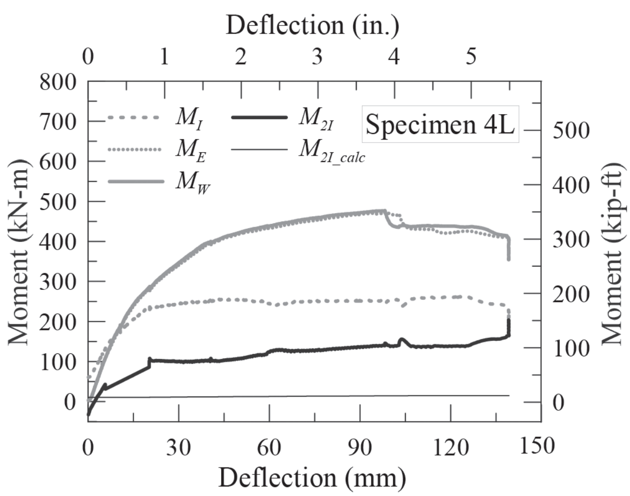


*(b) Internal moment-deflection curves of Specimen 4L*

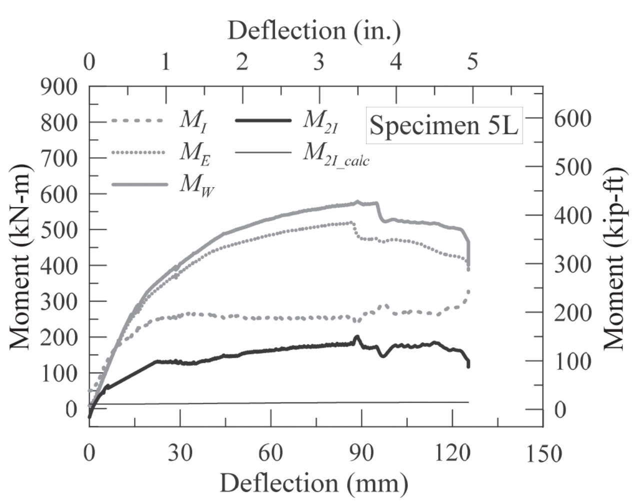


*(c) Internal moment-deflection curves of Specimen 5L*

*Fig. 14—Internal moment-deflection curves at critical sections and secondary (internal) moment.*

The assumption was that plastic moment capacity was developed at the interior support. Here, the plastic hinging formation was apparent as the mild steel bars yielded as a great degree of cracking occurred (Fig. 15). Additionally, the total actuator load was equivalent or a bit larger than the capacity calculated, assuming that nominal moment strengths were reached at all four critical sections (including one left and one right of interior support). However, unlike the existing postulation, the bending resistance at the interior support location seemed to be achieved from a combination of two different mechanisms: by internal beam moment resistance and by hold-down force induced by the post-tensioning. Internally, unbonded PT beams appear to act like beams with external PT tendons as external loading is increased.

The secondary reaction and moment continuously increased as the external load increased, and at the same time the internal moment at the interior support location was kept almost constant until concrete crushing at midspan locations. No concrete crushing was observed to occur at the interior support even though plastic hinging was formed here much earlier than the other locations. Figure 15 seems to explain the reason for no compression failure at the interior support region. After substantial yielding of mild steel bars (that is, formation of plastic hinging), it was found that compressive strains in the bottom bars did not increase but decrease, possibly by the activation of hold-down force of unbonded tendons. At the same time, the tensile strains in the top bars were also quite restrained.

The finding in this paper is surprising. Conventional sectional analysis does not seem to be appropriate for indeterminate unbonded PT structures. The magnitude of negative moment capacity may not be too different from that from

**Table 2—Measured prestress loss due to elastic shortening from firstly jacked tendons**

| Specimen | 4H | 4L | 5L |
|---|---|---|---|
| Prestress loss, MPa | 11.3 | 27.5 | 35.3 |

Note: 1 MPa = 145 psi.

**Table 3—Secondary moment evaluated in two different approaches at peak load**

| Specimen | 4H | 4L | 5L |
|---|---|---|---|
| $M_{2I}$, kN-m | 134.3 | 139.6 | 183.9 |
| $M_{2I\_calc}$, kN-m | 13.1 | 14.6 | 17.2 |

Note: $M_{2I}$ is monitored secondary moment at interior support location; $M_{2I\_calc}$ is secondary moment at interior support location, which is evaluated using load-balancing method;1 kN-m = 738 ft-lb previous knowledge. The larger secondary hold-down force would be beneficial in terms of shear and punching shear resistance. However, required slab moment at midspan and axial force at end columns may be augmented by secondary effects because interior reactions tend to be reduced. It is highly recommended for other independent researchers to conduct similar tests and measure reaction forces until failure.

## SUMMARY AND CONCLUSIONS

Experimental studies on the flexural behavior of seven two-span unbonded PT concrete beams were carried out under four-point loading conditions. Secondary effect in unbonded PT beams is known to be produced by the prestressing force and restraint in statically indeterminate structures. This phenomenon was monitored and investigated in this paper, and primary observations are summarized as follows.

1. The prestress measured at the jacking and fixed ends and between them for three specimens with different tendon types, profiles, and prestressing forces showed almost the same variation trend when the member underwent the long-term prestress loss and external load increments. Also, variation observed was similar to the previous measurement under quasi-static loading by other researchers—the implication being that prestress along the length of continuous PT members may experience similar prestress variation trends.
2. The secondary moment estimated using experimental data varied depending on elastic and inelastic behavior stages, which significantly differed from the secondary moments calculated based on the indeterminate frame analysis and load-balancing method. The secondary moments were increased with increasing external load, and in the post-elastic stage, their values were significantly larger than the calculated values. Larger hold-down force at interior support appeared to be a part of bending resistance along with internal beam moment resistance. Unbonded PT beams appear to behave quite differently from bonded systems.
3. The measured total actuator load exceeded the plastic capacity of the whole member calculated through the plastic analysis theory, where the nominal moment strengths were assumed to be reached at all critical sections. Conversely, secondary moment at midspan and secondary column axial force may be larger than expected at ultimate limit state. No design changes are suggested at this time but may be necessary in the future with extensive further research.
4. By comparing paired specimens (4H and 4L; 4L and 5L), it was noted that the secondary moment tended to be larger when the specimen had the higher tendon profile and larger prestressing force.

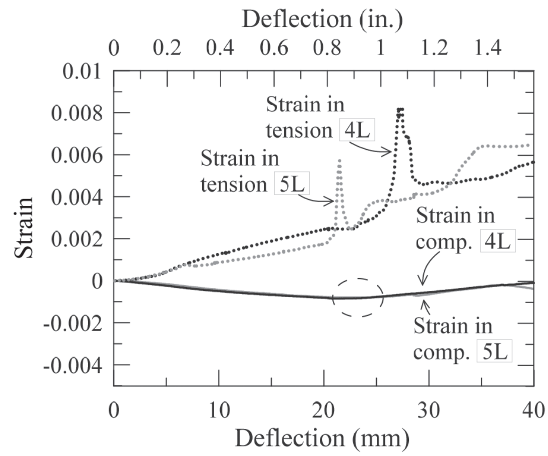


*Fig. 15—Strain deflection curves at section of interior support location (Specimens 4L and 5L). (Note that 0.002 is approximately the yield strain for mild steel with specified yield strength of 400 MPa.)*

## ACKNOWLEDGMENTS

The authors would like to thank financial support by the National Research Foundation of Korea (Grant No. 2018R1D1A1B06044752) and by POSCO.

## REFERENCES

ACI Committee 318, 1971, "Building Code Requirements for Reinforced Concrete (ACI 318-71)," American Concrete Institute, Farmington Hills, MI, 78 pp.

ACI Committee 318, 1977, "Building Code Requirements for Structural Concrete (ACI 318-77)," American Concrete Institute, Farmington Hills, MI, 103 pp.

ACI Committee 318, 2014, "Building Code Requirements for Structural Concrete (ACI 318-14) and Commentary (ACI 318R-14)," American Concrete Institute, Farmington Hills, MI, 520 pp.

Bondy, K. B., 2003, "Moment Redistribution: Principles and Practice Using ACI 318-02," *PTI JOURNAL*, V. 1, No. 1, pp. 5-23.

Burns, N. H., and Pierce, D. M., 1967, "Strength and Behavior of Prestressed Concrete Members with Unbonded Tendons," *PCI Journal*, V. 12, No. 5, pp. 15-29.

Burns, N. H.; Helwig, T.; and Tsujimoto, T., 1991, "Effective Prestress Force in Continuous Post-Tensioned Beams with Unbonded Tendons," *ACI Structural Journal*, V. 88, No. 1, Jan.-Feb., pp. 84-90.

Cohn, M. Z., and Frostig, Y., 1983, "Nonlinear Analysis of Continuous Prestressed Concrete Beams," *International Symposium—Nonlinearity and Continuity in Prestressed Concrete*, V. 2, University of Waterloo, Waterloo, ON, Canada, pp. 45-76.

Harajli, M.; Mabsout, M. E.; and Al-Hajj, J. A., 2002, "Response of Externally Post-Tensioned Continuous Member," *ACI Structural Journal*, V. 99, No. 5, Sept.-Oct., pp. 671-680.

Hufnagel, A., and Kang, T. H.-K., 2012, "Assessment of Secondary Effects in Post-Tensioned Flat Plates," *PTI JOURNAL*, V. 8, No. 2, pp. 26-42.

KCI, 2012, *KCI-12: Concrete Structure's Code*, Korea Concrete Institute, Seoul, Korea. (in Korean)

Lee, S.-H.; Shin, K.-J.; and Kang, T. H.-K., 2015, "Flexural Strengthening of Continuous Concrete Beams Using Externally Prestressed Steel Bars," *PCI Journal*, V. 60, No. 1, pp. 68-86.

Lin, T. Y., 1955, "Strength of Continuous Prestressed Concrete Beams under Static and Repeated Loads," *ACI Journal Proceedings*, V. 51, No. 6, June, pp. 1037-1059.

Maguire, M.; Collins, W. N.; Halbe, K. R.; and Roberts-Wollmann, C. L., 2016, "Multi-Span Members with Unbonded Tendons: Ultimate Strength Behavior," *ACI Structural Journal*, V. 113, No. 2, Mar.-Apr., pp. 195-204.

PTI Committee M-50, 2000, "Anchorage Zone Design (PTI M50.2-00)," Post-Tensioning Institute, Farmington Hills, MI.

Wyche, P. J.; Uren, J. G.; and Reynolds, G. C., 1992, "Interaction between Prestress Secondary Moments, Moment Redistribution, and Ductility—A Treatise on the Australian Concrete Codes," *ACI Structural Journal*, V. 89, No. 1, Jan.-Feb., pp. 57-70.

***Kyungmin Kim*** *is a former Master's Student at Seoul National University, Seoul, Korea. Currently he is working as a structural engineer at T-Sec Group. He received his BS from Hanyang University, Seoul, Korea and his MS from S eoul National University. His research interests include design and behavior of reinforced and post-tensioned concrete structures.*

*PTI Fellow* ***Thomas H.-K. Kang*** *is a Professor at Seoul National University, Seoul, Korea. Before that, he was an Assistant Professor at the University of Oklahoma. He is a licensed professional engineer in California. He received his BS from Seoul National University and his PhD from the University of California, Los Angeles, Los Angeles, CA. He is a member of PTI Committee DC-20, Building Design.*